Ocean Modelling 30 (2009) 143–154

Contents lists available at ScienceDirect

Ocean Modelling

journal homepage: www.elsevier.com/locate/ocemod

Assimilation of historical SST data for long-term ENSO retrospective forecasts

Xiaobing Zhou [1], Youmin Tang *, Ziwang Deng

Environmental Science and Engineering, University of Northern British Columbia, 3333 University Way, Prince George, BC, Canada V2N 4Z9

ARTICLE INFO

Article history:
Received 15 April 2008
Received in revised form 15 June 2009
Accepted 19 June 2009
Available online 25 July 2009

Keywords:
ENSO
Retrospective forecast
Data assimilation
Background error covariance

ABSTRACT

In this study, the assimilation of historic SST (sea surface temperature) data was performed for long-term ENSO hindcasts. The emphasis was placed on the design of background error covariance (BEC) that dominates the transfer of SST information to the subsurface. Four different data-assimilation schemes, based on Optimal Interpolation (OI) algorithm, were proposed, and compared in terms of ENSO simulation and prediction skills for the period from 1876 to 2000.

It was found that the data-assimilation scheme that has a three-dimensional BEC constructed from model simulations forced by observed wind stress can effectively correct the second-layer temperature in the SST assimilation and lead to the best ENSO prediction skill. Further analysis for the long-term hindcasts shows that the prediction skills have a striking decadal/interdecadal variability similar to that found in other models. These results provide a fundamental basis for the further study of ENSO predictability.

1. Introduction

The El Niño-Southern Oscillation (ENSO), a fluctuation between warm (El Niño) and cold (La Niña) conditions in the tropical Pacific, is the most prominent year-to-year climate variation on the Earth. ENSO originates in the tropical Pacific through interactions between the ocean and the atmosphere, but has both local and global impacts on environment and socioeconomic conditions.

ENSO predictability is one of key issues in ENSO study. A widely used strategy for this research is to perform hindcast experiments using dynamical models, by which the variations of predictability and the causes responsible for the variations are examined. So far, most of hindcasts performed by dynamical models generally cover a period of around 20–40 years due to the fact that long-term observational records of forcing data (such as wind stress) are not available. Therefore, the period available to test the predictability covers few ENSO cycles, basically precluding statistically robust conclusions.

For a complete examination of ENSO predictability, long-term hindcasts that can cover sufficient ENSO cycles are required. Chen et al. (2004) made the first effort towards this goal. They used Lamont model (Zebiak and Cane, 1987; Cane et al., 1986) to perform hindcasts of the past 148 years from 1856 to 2003 initialized by Kaplan's reconstructed SST data (Kaplan et al., 1998). They found that the ENSO predictability shows clearly decadal variations with high skill in the late 19th and 20th century.

ENSO prediction skill is usually model dependent, thus it is of interest to examine the variation of ENSO predictability in a general framework using more models. To perform a long-term hindcast with physical models, especially with hybrid coupled models composed of statistical atmosphere and dynamical ocean, there are two central issues: (1) extending forcing data (e.g., wind stress) using long-term datasets available; (2) retrospective forecasts initialized by assimilating historic SST that is probably an only oceanic dataset of over 100 years. The first issue, which can be found in Deng and Tang (2009) in detail, will be briefly introduced in Section 3. In this paper, we will address the second issue, i.e., the assimilation of the historic SST dataset. This work attempts to provide an effective assimilation scheme for SST, leading to skilful hindcasts for a long period.

SST is usually a prognostic variable in ocean models. A direct strategy to assimilate SST is to insert it into ocean models by a specified algorithm. However it was often found that this direct strategy can produce serious imbalance between surface and subsurface, leading to poor prediction skills (Chen et al., 1997; Rosati et al., 1997; Tang and Hsieh, 2003). Therefore, an important issue is how to correct model's subsurface temperature when assimilating SST observations. The subsurface temperature has a long memory for coupled systems and is important for ENSO predictions of long lead times beyond 6 months. The nudging scheme used in a framework of coupling assimilation may be able to avoid the imbalance induced from SST assimilation through turning nudging parameters, producing good initial conditions for ENSO predictions (e.g., Keenlyside et al., 2005; Luo et al., 2005).

In this study, we will address the construction of background error covariance (BEC). The BEC plays a vital role in data assimilation, since it dominates information distribution in space and

* Corresponding author. Tel.: +1 250 9605190; fax: +1 250 9605845.
E-mail address: ytang@unbc.ca (Y. Tang).
[1] Present address: Centre for Australian Weather and Climate Research (CAWCR), Bureau of Meteorology, 700 Collins St, Melbourne, Vic. 3001, Australia.

1463-5003/$ - see front matter © 2009 Elsevier Ltd. All rights reserved.
doi:10.1016/j.ocemod.2009.06.015

among variables. With a well-defined BEC, one can expect that the observed SST information can be spread into the deep ocean, thereby correcting the subsurface temperature.

The assimilation algorithm used here is the Optimal Interpolation (OI) method, which has been widely applied in atmospheric and oceanographic data assimilation. OI is a least square optimal estimate that can be analytically solved and is easy to implement. One of its disadvantages is the costly expense for high dimensional problems due to large dimensional covariance matrices. In addition, the OI cannot deal with nonlinear observation operators. In the present study, however, our ocean model only covers the tropical Pacific domain, and the observation operator is bilinear. In particular, this study addresses the propagation of SST increments to the subsurface through BEC. Thus, a simple assimilation algorithm like OI. can be chosen based on the above considerations.

Like variational data assimilation, OI needs a prescribed BEC in the assimilation cycle. At present, there are several approaches to construct the BEC. Hollingsworth and Lonnberg (1986) (HL) proposed a method which looks at the spatial covariance of the differences between observations and the background. The HL method has the advantage that is a direct diagnosis of background error covariance. However, it requires a uniform set of unbiased observations with spatially uncorrelated errors. Unfortunately, oceanic observations are sparse and even unavailable in the deep ocean. In addition, the ocean model used here, which will be described in the next section, is a simplified dynamical model. The model's subsurface temperature does not match the real observations at the same depth. Therefore, even if there were enough subsurface temperature observations, it would still be difficult to use the HL method to calculate the BEC for our model.

In weather forecasting, the NMC (National Meteorological Center, nowadays named National Center for Environmental Prediction) method (Parrish and Derber, 1992) and the analysis-ensemble method are commonly used to estimate the model BEC in addition to the HL method (Fisher and Courtier, 1995). The NMC method assumes that the statistical structure of forecast errors varies little over 48 h. Under this assumption, the spatial correlations of background error should be similar to the correlations of differences between 48 and 24 h forecast verifying at the same time.

In the ocean data assimilation, Derber and Rosati (1989) adopted an empirical formula-traditional Gaussian function for the BEC with given spatial correlation scales. Behringer et al. (1998) further modified the method of Derber and Rosati (1989) by considering the anisotropy in zonal and meridional directions. Weaver and Courtier (2001) described a practical algorithm that can be used to model correlation functions on the sphere. These BECs are Gaussian-type functions where the correlations are weighted by the separate latitudinal and longitudinal distances. One critical problem in these methods is how to determine the spatial correlation scales. Zhou et al. (2004) estimated the horizontal scales of model temperature errors based on the outputs of a tropical Pacific Ocean model. They fitted a Gaussian function to the correlation coefficients between model grid points via a nonlinear fitting approach. Using such spatial correlation scales and two-dimensional variational assimilation (2D-Var), they found the differences of the annual-mean temperature between model and observation to be greatly reduced compared to the results of the control run. Oke et al. (2005, 2008) also estimated BECs using model ensemble. A tuning parameter α was used in their scheme to adjust the magnitude of BECs. In addition, Borovikov et al. (2005) and Alves and Robert (2005) estimated BECs using a Monte Carlo simulation by perturbing surface wind stress.

In this study, we further developed the method of BEC used in Zhou et al. (2004) for SST assimilation. Two major improvements were made. First, the location-dependent vertical correlations of model error are considered, which was ignored in Zhou et al. (2004); Second, Zhou et al. (2004) used model original temperature to estimate the spatial correlation scales of errors. Here we use a derivative of the model temperature anomalies to estimate the BEC. This will be described in Section 3.2. On the other hand, Zhou et al. (2004) considered the model annual-mean temperature, whereas we address the interannual variation of temperature.

This paper is organized as follows: the model, observations and the construction of wind stresses will be introduced in Section 2; four assimilation schemes will be proposed in Section 3; in Section 4, the ocean analyses of the four schemes will be presented for the period from 1876 to 2000; the results of hindcasts for 125 years from 1876 to 2000 will appear in Section 5, followed by a discussion and conclusion in Section 6.

2. The model, the data and the construction of wind stresses

The hybrid coupled model (HCM) used in this study is composed of a nonlinear dynamical ocean model and a nonlinear empirical atmospheric model. The ocean model is an intermediate complexity model, derived from Anderson and McCreary (1985) and Balmaseda et al. (1994, 1995) and extended to six active layers (Tang et al., 2001). It covers the tropical Pacific Ocean 30°N–30°S in latitude and from 123°E–69°W in longitude with a horizontal resolution of $1.5^\circ \times 1.5^\circ$, and consists of the depth averaged primitive equations in six layers (with reference thickness of 100, 175, 250, 320, 400 and 500 m from top to bottom). The time step for integration is 2 h. The model allows for exchange of mass, momentum and heat at each layer interface by a parameterization of entrainment.

The atmospheric model is built by the nonlinear regression method, via a neural network (NN) approach (Tang et al., 2001). The wind stress is reconstructed using ocean states as predictors. The coupling is done once every 15 days in this study. We found that ENSO prediction skill was insensitive to the coupling time interval when it ranges from one to 15 days, probably because the atmospheric model was constructed using monthly mean data. The details of the oceanic and atmospheric model can be found in Tang et al. (2001) and Tang (2002).

Two observation datasets are used in this study. One is ERSST (Extended Reconstructed SST) data. Its horizontal resolution is $2^\circ \times 2^\circ$ over the global ocean (Smith and Reynolds, 2003, 2004). The data period used here is from 1876 to 2002. It has the largest uncertainty in the nineteenth century and during the two world wars due to sparse sampling. The uncertainty of its global average is, at the confidence level of 95%, around 0.4 °C in the 19th century, near 0.2 °C for the first-half of the 20th century and 0.1 °C or less after 1950. This dataset has been widely used in climate studies (Xue et al., 2003; Monahan and Dai, 2004; Nakaegawa et al., 2004). The other dataset is the NCEP (National Centers for Environmental Prediction) reanalysis monthly wind data for the period from 1948 to 2002. Its resolution is the same as that of ERSST data.

To perform a long-term simulation and hindcast of ENSO, the past wind stress data, as the model forcing, is required. Using SST as a predictor and SVD technique, a long-term wind stress dataset from 1875 to 1947 was reconstructed, with the resolution $2^\circ \times 2^\circ$ and the domain of tropical Pacific from 30°S–30°N (see http://web.unbc.ca/ytang/wind.html). The cross-validation scheme was used in the reconstruction to ensure the training data not used in test periods. The training data of the wind is the NCEP reanalysis 10 m wind speed in monthly T62 Gaussian grids for 1948–2006 (Kalnay et al., 1996). A detailed description on the reconstruction of wind stress was given in Deng and Tang (2009). With the reconstructed wind stress, a long-term control run was performed with the OGCM from 1876 to 2000, producing a good simulation for ENSO variability as discussed later. In next sections, the perfor-

mances of assimilation schemes will be evaluated through comparisons against this control run.

3. Data-assimilation schemes

The OI algorithm used in this study is a real-time assimilation method where the optimal state is given by the Best Linear Unbiased Estimate (BLUE). In principle, it can be written as,

$$x_a = x_b + K(y - H[x_b]), \tag{1}$$

$$K = BH^T(HBH^T + R)^{-1}, \tag{2}$$

where x_a is analyzed model state, x_b is background model state, y is the observed SST, H is observation operator, B is covariance matrix of background errors, R is the covariance matrix of observation errors. The linear operator K is called Kalman gain. In (2), the BEC matrix B describes the spatial and multivariate structure of the analysis increment, and plays a critical role in the data-assimilation system.

The observed SST used for the assimilation is ERSST SST dataset. These data are also used to construct a proxy-SST dataset for Scheme 4. The goal and method using a proxy data instead of original SST will be presented in Scheme 4. The data are inserted each 5-day into the model with a weighted coefficient that is determined by the distance between the model time and the time used to represent monthly observed SST value (i.e., the 15th day of each month).

The matrix B in (2) can be written

$$B = \begin{pmatrix} B_{11} & B_{12} \\ B_{21} & B_{22} \end{pmatrix}, \tag{3}$$

where sub-matrices B_{11} and B_{22} stand for the background error covariance of model SSTA T_1 and the second-layer temperature anomaly T_2, respectively; B_{12} and B_{21} represent the error cross-covariance between the T_1 and T_2. B_{12} is equal to B_{21}. Actually B_{22} is not used here, since only SST data is assimilated into the ocean model and no subsurface temperature data is available for a 125-year period. B should be a positive-definite and symmetric matrix. Here, we would not expect SST to correlate with temperatures below the second-layer, since the reference depth of the first-two layers of the ocean model is 270 m, which is far beyond the thermocline that dominates ENSO variability. The objective of this study is to provide a good initialization scheme for ENSO forecasts.

Four different schemes of data assimilation are proposed below. In the first-two schemes, we consider a two-dimensional assimilation as Derber and Rosati (1989), Behringer et al. (1998) and Tang et al. (2004). Both schemes have only non-zero element of B_{11} in BEC matrix, and ignore error covariance in vertical, thereby failing to transfer the SST increments to the subsurface. For the latter two schemes, we consider errors in vertical correlation in the BEC, allowing information transfer between the SST and the second-layer temperature. In these two cases, besides B_{11}, B is a matrix with non-zero values for B_{12} (B_{21}). B_{22} is always not used due to the absence of subsurface observed temperature.

The observational error covariance matrix R should be estimated not only from measurement errors but also from errors of representativeness (e.g., Lorenc, 1986). The latter reflects the fact that the forward model, which maps the model state to the observed variables and locations, is not perfect. The ERSST SST datasets used here are ship reports or binned raw observations. It is difficult to estimate the R matrix. In general, the area which has a large variability is usually accompanied by a large error such as in the regions of western boundary currents and thermocline etc. (Martin et al., 2007; Behringer et al., 1998). Therefore, one can assume that the standard deviation of the observed SSTA errors is proportional to the standard deviation of observed SSTA. For simplicity, the observed errors here are also assumed to be uncorrelated in time and space as in Tang and Kleeman (2002) and Tang and Hsieh (2003).[2] It should be noticed that the real observed temperature errors should be correlated each other. The problem is that it is difficult to estimate their correlation structure. Thus, for simplicity, R has values of zero everywhere except diagonal elements which are equal to

$$r_i = (\beta\sigma_o(i))^2, \tag{4}$$

where β is a tuning parameter, set to be 0.3 in this study, σ_o is the standard deviation of observed SSTA (Fig. 1b).

3.1. Scheme 1

In this scheme, the model BEC B_{11} is assumed to be a simple Gaussian function with the homogeneous and isotropic assumption and ignores vertical correlations as in Derber and Rosati (1989). The horizontal covariance between any two points is given by

$$b_{ij} \approx ae^{-d_1^2(i,j)/(d^2\cos\phi)}, \tag{5}$$

where b_{ij} is any element of B_{11} in (2), ϕ is the latitude of the grid point, $d_1(i,j)$ the distance between any two points in the model domain, $a = 0.01$, and $d = 570$ km, as in Derber and Rosati (1989).

The observational SST errors are assumed to be non-correlated in time and space, so the observation error covariance matrix is diagonal and its error variance is set to $(0.5^\circ C)^2$ as some previous studies (e.g., Tang et al., 2004).

3.2. Scheme 2

In this scheme the BEC B_{11} is estimated from the modeled SST at each grid point instead of a pre-described Gaussian function of Scheme 1. The monthly model SST is obtained by integrating the ocean model for 21 years from 1980 to 2000 forced by the observed wind stress.

An specific element in B_{11} is given below

$$b_{ij} = \frac{1}{N-1}\sum_{n=1}^{N}\left\{\left[T_1'^n(i) - \overline{T}_1'(i)\right] * \left[T_1'^n(j) - \overline{T}_1'(j)\right]\right\}, \tag{6}$$

where N is the number of samples ($N = 21 * 12$), $\overline{T}_1'(i)$ is the mean of T_1', and $T_1'^n(i)$ is defined below

$$T_1'^n(i) = \frac{T_1^n(i)}{\sigma_1(i)}\sigma_{om} \tag{7}$$

where $T_1^n(i)$ is the model SSTA at grid point i and sample n, $\sigma_1(i)$ is the standard deviation of model $T_1(i)$ during the period 1980–2000, and $\sigma_{om}(i)$ indicates root mean square (RMS) between the model $T_1(i)$ and the observed SSTA $T_o(i)$ (Fig. 1a), namely

$$\sigma_{om}(i) = \sqrt{\frac{1}{N-1}\sum_{n=1}^{N}\left(T_1^n(i) - T_o^n(i)\right)^2} \tag{8}$$

The observed SSTA is interpolated to each model grid prior to the computation of $\sigma_{om}(i)$.

In (6), $T_1'^n(i)$ is used to define B_{11} since we want the variance of model error (i.e., the diagonal elements of B_{11}) is equal to the square of $\sigma_{om}(i)$. Under the assumption that the observed SSTA is an unbiased estimate of its true value, the square of $\sigma_{om}(i)$ is identical to the variance of model errors. $B_{12} = 0$ in Schemes 1 and 2.

[2] The historic SST dataset is a reconstructed data, thus this assumption might not hold as well as that in other studies where the real observations were used.

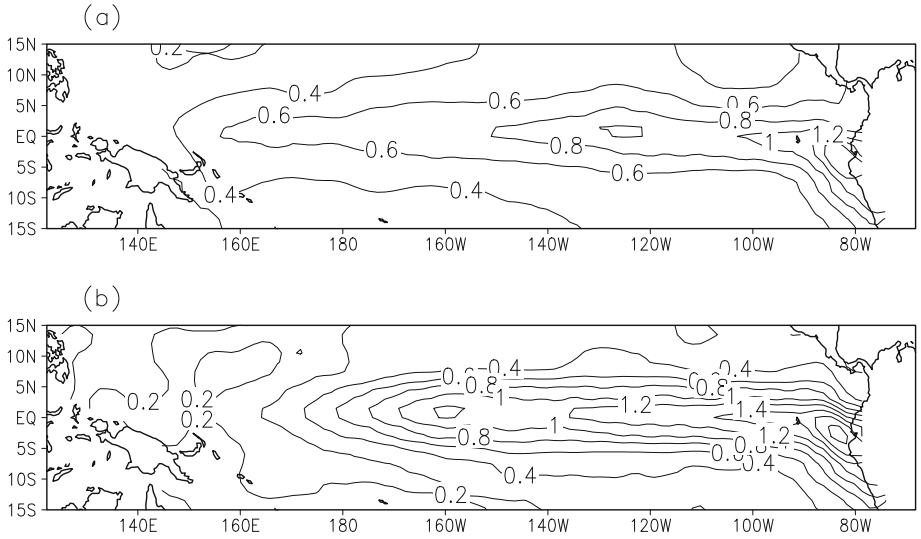

Fig. 1. (a) The RMSE between the modeled SSTA and observed SSTA during the period 1980–2000. The ocean model was forced by FSU wind stress; (b) the standard deviation of observations SSTA (unit: °C).

3.3. Scheme 3

In this scheme, B_{11} is exactly same as that in Scheme 2. The estimate of B_{12} is similar to that of B_{11}. Like (7), $T_2'^n$ can also be written,

$$T_2'^n(i) = \frac{T_2^n(i)}{\sigma_2(i)}\sigma(i), \tag{9}$$

where $T_2^n(i)$ is the second-layer temperature anomalies at model grid point i and sample n, $\sigma_2(i)$ is the standard deviation of $T_2(i)$ during the period of 1980–2000, $\sigma(i)$ is the standard deviation of the second-layer temperature errors. Since the ocean model used here is a simplified dynamical model, the model $T_2(i)$ does not match the observed temperature at the same depth. Thus $\sigma(i)$ is here assumed to be 0.1 at any model grid point, as suggested in Derber and Rosati (1989). Similar to (6), an element of sub-matrix B_{12} can be written as,

$$b_{i,j} = \frac{1}{N-1}\sum_{n=1}^{N}\left\{\left[T_1'^n(i) - \overline{T}_1'(i)\right] * \left[T_2'^n(j) - \overline{T}_2'(j)\right]\right\}, \tag{10}$$

where $\overline{T}_1'(i)$ and $\overline{T}_2'(j)$ represent the mean value of $T_1'(i)$ and $T_2'(j)$, respectively. The term B_{12} in (3) transfers information of the sea surface temperature to the second-layer temperature.

Fig. 2 shows several correlation structures of temperature anomalies obtained using two reference locations in the first-layer. One location is in the western Pacific (168.5°E, 3°N) for Fig. 2a and b, and the other one in the eastern Pacific (240.5°E, 3°N) for Fig. 2c and d. Fig. 2a and c are spatial correlation structures for the first-layer itself whereas Fig. 2b and d are cross-correlation structures for different layers, namely the reference location in the first-layers correlated with all grids in the second-layer. As can be seen, the zonal correlation length scale is much larger than the meridional counterpart, consistent with the findings in Behringer et al. (1998) and Zhou et al. (2004). The zonal correlation length scale (Fig. 2a and c) reaches thousands of kilometres, because this simplified ocean model is dominated by large-scale dynamics due to shallow-water approximation. Fig. 2b and d suggest a teleconnection structure between the first-layer and the second large, as shown by high correlation values away from the reference locations. Interestingly, the large correlation values distribute along the off-equatorial belt around 5°–10°N/S in Fig. 2b and d, suggesting the importance of Rossby waves in the heat transfer in the vertical direction.

3.4. Scheme 4

In Schemes 1–3, the ERSST SSTA data are directly assimilated into the ocean model. In this scheme we attempt to assimilate a proxy-SST dataset into the model. Tang and Kleeman (2002) argued that the observational forcing must not be made too strong in the region where the model has a significantly different structure of variance from the observation. Otherwise the model experiences a shock due to the SST assimilation, leading to serious imbalance between surface and subsurface. To solve this issue, Tang and Kleeman (2002) proposed a strategy, namely assimilating an observed SST-induced proxy dataset instead of original observations. However, Tang and Kleeman (2002) did not consider B_{12} in their assimilation scheme, i.e., $B_{12} = 0$ in the error covariance matrix. It is interesting to explore whether the proxy-data strategy is still helpful if B_{12} is considered in SST assimilation, as proposed in Scheme 3. For this goal, we design a new scheme, namely, the formulation of background error covariance B is the same as that defined in Scheme 3 but using the proxy data instead of the original SST observations.

The proxy data is constructed through the time series of the first-three Empirical Orthogonal Functions (EOF) modes of the observed SST multiplied by the corresponding spatial patterns of the modeled SST field from the control run during 1964–2000. As argued in Tang and Kleeman (2002), the proxy SST data keeps the observation information in time but avoids large differences of spatial patterns of variances between observed SST and model SST. Besides the proxy SST data, a proxy data of the first-layer depth was also assimilated into the model with the BEC scheme identical to that in Scheme 1, i.e., ignoring the vertical covariance.

4. Ocean analyses

First we will examine ENSO simulations using reconstructed wind stress data with and without data assimilation. The anomaly correlation and RMSE between the observed and modeled SSTA during the period 1876–2000 are displayed in Fig. 3. In the control experiment, the good correlation skill only appears in the eastern-central equatorial Pacific. The poor skill of SSTA simulation in the western Pacific is probably due to poor parameterization of heat flux, which determines SST variations there (Shinoda and Hendon, 1998). It should be noticed that the poor simulation skill of SST in

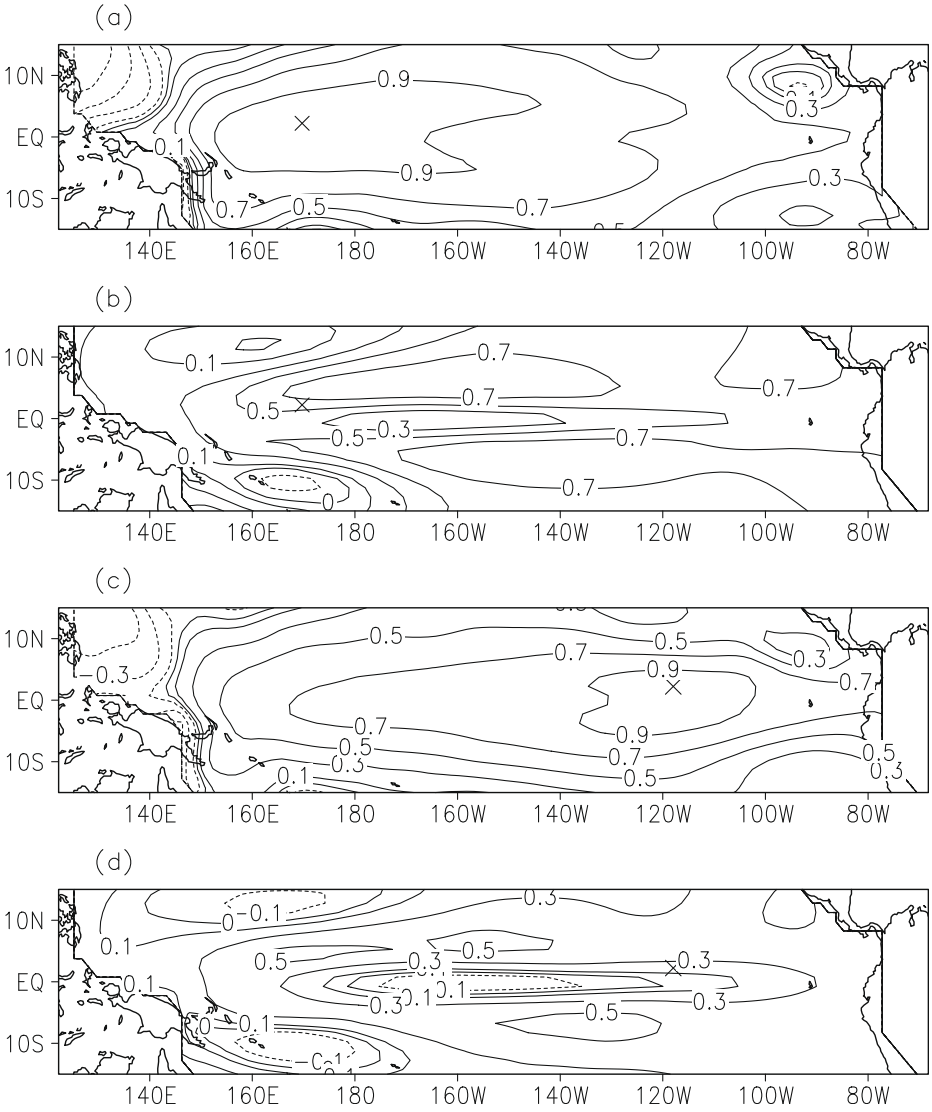

Fig. 2. Several correlation patterns for temperature anomalies derived from the ocean model 20-year run forced by FSU wind stress. Crosses mark the reference grid located in the first-layer that was here used to calculate the correlations. (a) and (c) are the correlations between the reference grid and all grids in the first-layer. (b) and (d) are the cross-correlations between the reference grid and all grids in the second-layer.

the western Pacific is not due to the quality of wind stress. In many oceanic models including some OGCMs (Oceanic General Circulation Model), the simulation skills of SSTA are also poor in the western Pacific Ocean, even though observed winds were used as model forcing data (e.g., Kug et al., 2005; Tang et al., 2004). In fact, the cross-validation skill showed that there is no significant difference of the quality in the reconstructed wind stress between the western Pacific and the eastern Pacific (Deng and Tang, 2009).

As be seen in Fig. 3, all assimilation schemes improve the SSTA simulation skills considerably. It is not surprising that such a high correlation is achieved, because the SSTA observations that were assimilated into ocean model are used again to measure the simulation skills. Schemes 2 and 3 have almost the same simulation skills, since they share the same BEC and observation error variances. However, their simulation skills of SSTA have considerably pronounced differences with Schemes 1 and 4 in the western Pacific. This is because Schemes 2 and 3 consider local-dependence of error correlation length scale, and use actual observation data. In Scheme 1 the correlation length scale in BEC is a constant value of 570 km everywhere whereas in Scheme 4 the SST-induced proxy data were assimilated into the oceanic model. The proxy data were reconstructed based on the first-three model EOF patterns, which account for major variances in the eastern tropical Pacific, thus leading to low skills in the western Pacific.

Fig. 4a and b show the time evolution of observed and modeled Niño3 (5°S–5°N, 120°–170°W) SSTA from January 1876 to December 2001 derived from the control run and Scheme 3, respectively. The anomaly correlation between the observed and modeled Niño3 SSTA is 0.89 in control run and 0.98 in Scheme 3. Fig. 4 suggests that (1) the reconstructed wind stress can facilitate the realistic interannual variability. As such the model forced by the reconstructed wind stress can capture all large ENSO events in both phase and amplitude; (2) the method of SST assimilation proposed in Scheme 3 is effective, making the model not only capture large events but many small events. Again, this is not surprising since the observed SST was assimilated into the model. Next we will explore the impact of SST assimilation on the subsurface oceanic analyses.

The major differences between Schemes 1, 2 and Schemes 3, 4 are that the former only correct model SST whereas the latter correct both the SST and the second-layer temperature (T2). We examined the differences of T2 anomalies between Schemes 1, 2

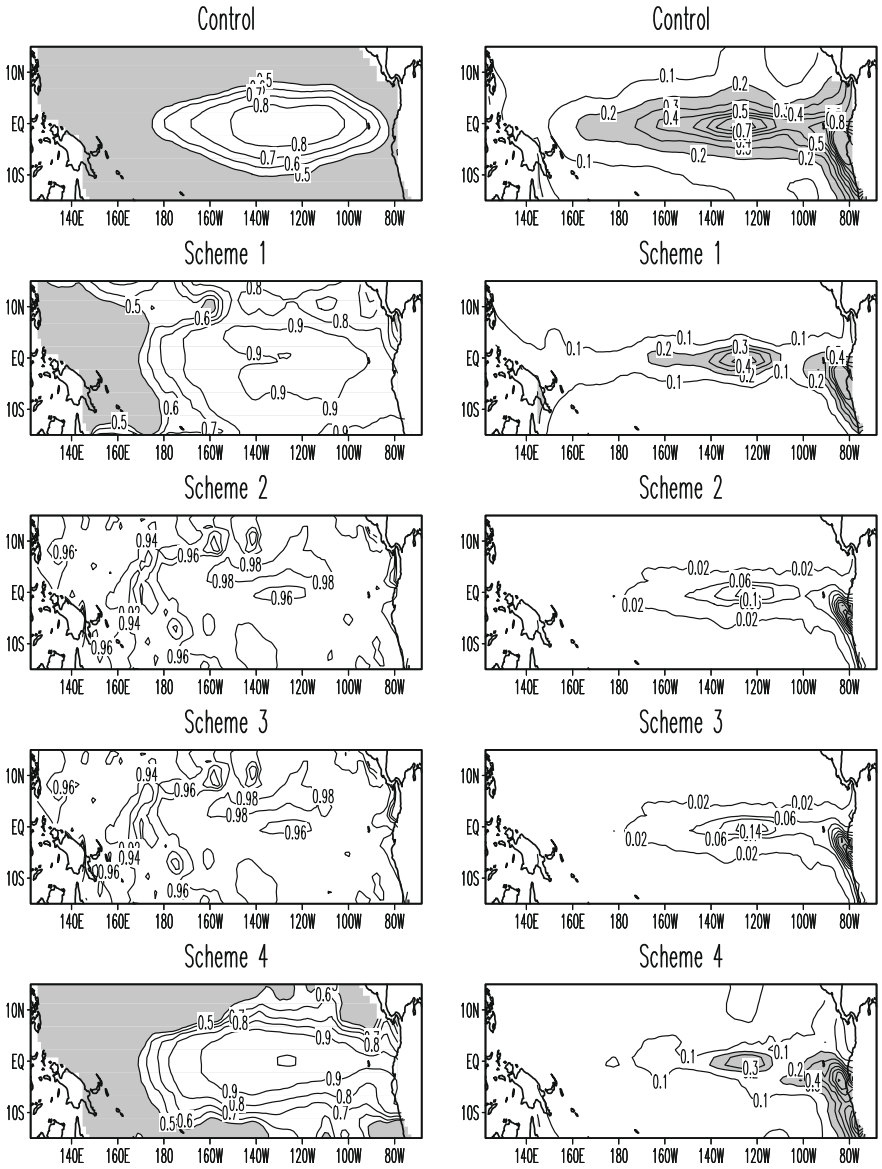

Fig. 3. Correlations (left panels) and RMSE (right panels) of modeled SSTA from the control experiment and the ocean analyses of four data-assimilation schemes, against the observed SSTA for the period from January 1876 to December 2000. The areas with correlation below 0.5 and RMSE above 0.2 °C are shaded.

with the control experiment, and found the differences are very subtle (not shown), indicating that the SST assimilation without considering vertical structure in BEC cannot effectively correct T2. This also suggests the inefficiency in transferring information of observed SST to the subsurface by the model itself. Thus, ignoring the vertical structure of BEC in SST assimilation could lead to serious imbalance between surface and subsurface.

Fig. 5a and b are the time-longitude plots of T2 anomalies along the equator from 1980 to 2000 for the control experiment, Schemes 3 and 4, respectively. As can be seen, Scheme 3 displays a significant eastward propagation during the El Niño events such as 1982/83 and 1997/98 which is almost absent in the control run. The eastward propagation of subsurface heat is a dominant feature in ENSO evolution, which is also a major source contributing to ENSO predictability in many dynamical models (Tang, 2002; Tang and Hsieh, 2003). The other significant difference between Fig. 5a and b are that the amplitude of the T2 anomalies is much smaller in the control run than in Scheme 3. We also conducted a similar control run from 1981 to 2000, i.e., forced the ocean model with the observed winds. It was found that the T2 anomalies, when forced by the observed winds, have relatively large amplitudes (not shown). The difference of T2 anomalies between the two control runs suggest that the small amplitude in Fig. 5a is mainly due to the reconstructed winds lacking the components that are highly frequent and not-SST related. These components may be important in exciting oceanic vertical waves that play a crucial role in variations of the subsurface temperature, although they are probably negligible for SST. Fig. 5 indicates that the proposed schemes with considering the vertical structure of BEC can effectively correct the second-layer temperature. The variability of subsurface ocean in Scheme 4 (Fig. 5c) is less realistic than that in Scheme 3, because proxy SST data, a blend of model and observed SST data, is assimilated into the ocean model.

The ocean model used here is an intermediate complexity layer model, which has a relative coarse resolution in vertical direction. In addition, the model depth is a prognostic variable, varying with time and location. Thus, it is difficult to validate ocean analyses through comparing the model temperature at the second-layer against the observed counterpart. However one might be able to validate the subsurface assimilation by the heat content anomalies (HCA), an integral of the upper ocean temperature with the depths.

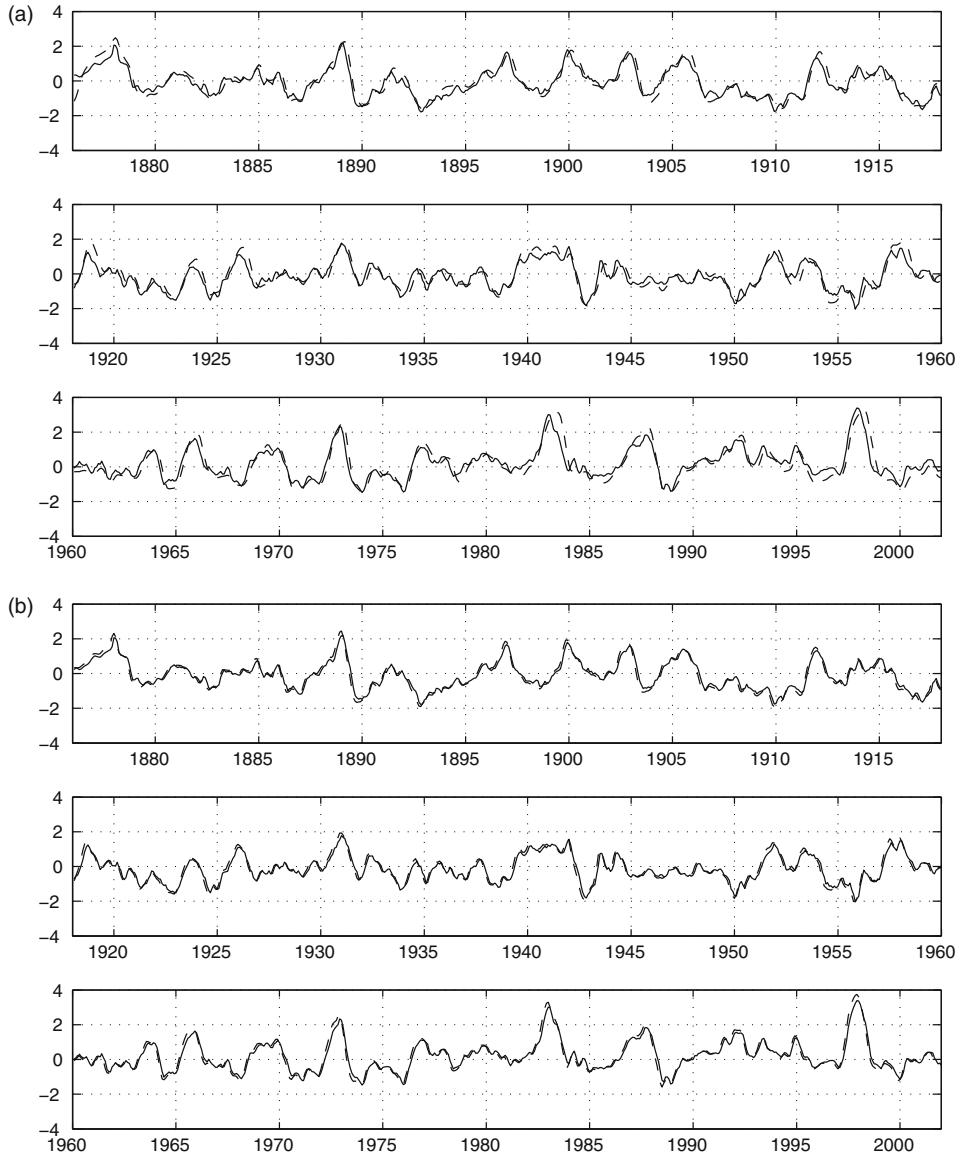

Fig. 4. Time-longitude plots of the heat content anomaly anomalies along the equator at top 270 m during 1980–2000 for (a) control run, (b) data assimilation of Scheme 3, and (b) NCEP reanalysis. The contour level is 0.3 °C in (a) and (B) and 1 °C in (c). The values over 0 °C are shaded.

Fig. 6 shows the time-longitude variation in HCA of the upper 270 m, along the equator, from the control experiment, Scheme 3 and NCEP (National Centers for Environmental Prediction) GODAS (Global Ocean Data Assimilation System) reanalysis dataset (Behringer et al., 1998) for the period from 1980 to 2000. As can be seen, the HCA simulation by Scheme 3 is better than that by the control run when compared against the NCEP reanalysis counterparts, especially for the strong ENSO events such as 1982/83 and 1997/98 El Niño events, although the amplitude of HCA analysis by Scheme 3 is still weak.

5. ENSO predictions

In this section, we will perform five groups of hindcasts using the HCM, initialized, respectively, from the control run and four different assimilation schemes described in Section 3. For each group of hindcast, a total of 500 prediction cases, initialized from April 1, 1876 to January 1, 2001, were run at three-month intervals (1 January, 1 April, 1 July and 1 October). Each prediction lasts 12 months. Fig. 7 shows predictive skills initialized from the control experiment and the assimilation schemes, where the predicted Niño3 SSTA index is compared against its observed counterpart. The correlation skill initialized from any data-assimilation scheme is higher than that from the control run, indicating that the initial conditions derived from any SST assimilation in this study can improve ENSO prediction skills. This is different from some previous work where the SST assimilation without considering the vertical structure in BEC led to poorer prediction skill (Chen et al., 1997; Rosati et al., 1997; Tang and Kleeman, 2002; Tang and Hsieh 2003). This is probably because there are relatively large initial errors in the model SST when the statistically reconstructed wind stress forced the ocean model, thereby leading to very low prediction skills for the control run. When the observed SST is assimilated into the model, the initial errors of SST are well corrected, especially in the western Pacific and in the off-equatorial region as shown in Fig. 3, leading to better prediction skill. It should be noted that the SST assimilation from Schemes 1 and 2, which do not consider vertical structure in BEC, could lead to imbalance between surface and subsurface, potentially degrading the prediction skill. Thus, Fig. 7 suggests that the impact of initial errors of SST on

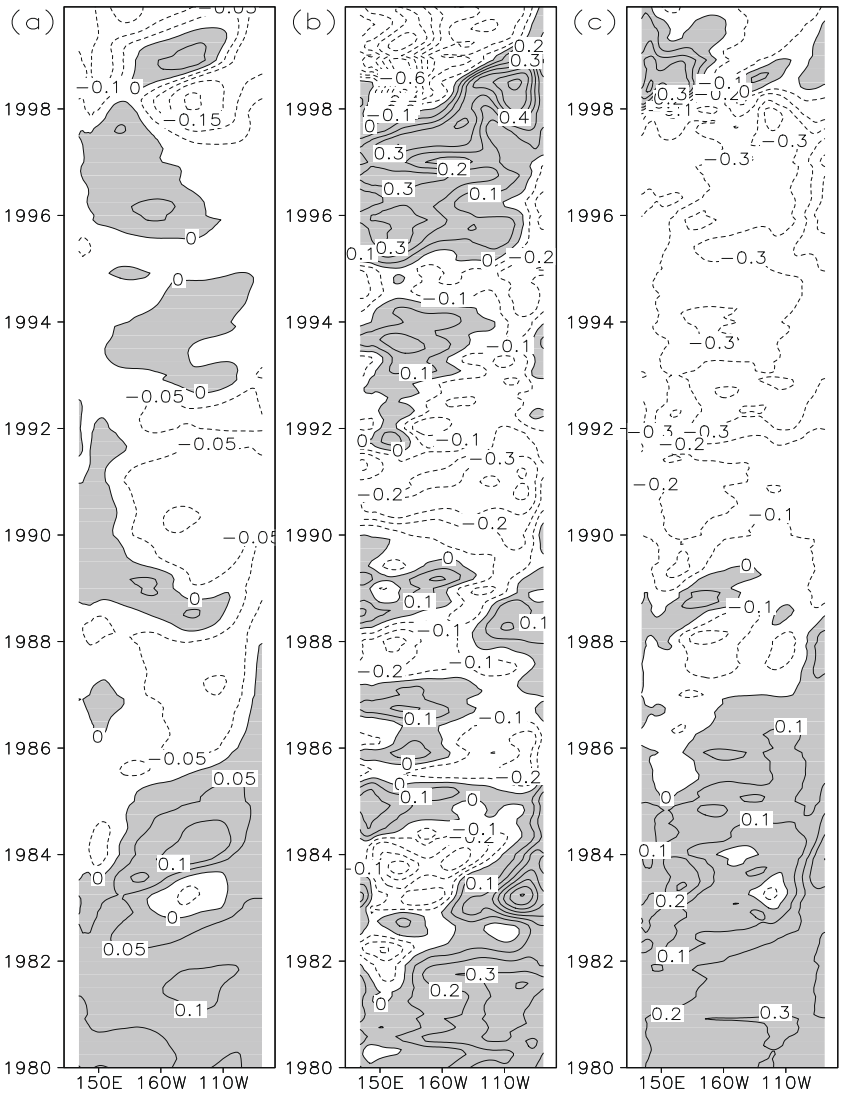

Fig. 5. Time evolution of observed (solid line) and modeled (dashed line) Niño3 SSTA from January 1876 to December 2001. The modeled values from the control run without data assimilation and from the oceanic analysis with Scheme 3 are shown in (a) and in (b), respectively. The correlation between observed and modeled Niño3 SSTA indices is 0.89 and 0.98 for the control run and data assimilation, respectively.

prediction skill might be much larger than that of the imbalance from the assimilation. The best overall predictive skills were attained in Scheme 3, especially for the prediction of lead times greater than 6 months. The correlation coefficients of predictions initialized by Scheme 3 are up to 0.5 at the 9-month lead whereas the skill initialized by the control run is below 0.5 at the lead times beyond 6 months. Generally, the prediction skill over correlation of 0.5 is supposed to be useful in ENSO community. Thus, the 'validity' of the forecast has been extended by 3–4 months by Scheme 3 compared with that by control run. It is also true for Nino3.4 SSTA prediction as shown in Fig. 8. In Schemes 3, the model SST and the second-layer temperature are corrected simultaneously, leading to better skills compared with skills in Schemes 1 and 2 where the only model SST is corrected. This indicates that the proposed BEC in Schemes 3 is effective in transferring correction from the surface to the subsurface. Scheme 4 also considers the correction of the second-layer temperature but a proxy-SST dataset used biased the realistic information assimilated into the model, leading to relatively small improvement in prediction skill.

Fig. 8 shows the variation in prediction skills of Niño3 SSTA index in different periods. For the first 20 years (1876–1895) and the last 60 years (1941–2000), the predictions of Niño3 SSTA index, when initialized by Scheme 3, are much better than those initialized by the control run, with the correlation skill of about 0.5 at the 12-month lead. During the period 1896–1940, the correlation skill from Scheme 3 is also better than that from the control run, but still much lower compared with the skills of other periods, especially for the prediction beyond 6-month lead. The low prediction skill during this period was also found in Lamont coupled model and a hybrid coupled model (Chen et al., 2004; Tang et al., 2008). This is the most probably due to relatively weak variability of ENSO during this period. The period with weak ENSO signals should be intrinsically less predictable because weak signals are easily dissipated by the chaotic or stochastic components of the system, leading to the loss of predictability. It has been argued that ENSO predictability is highly related to the strength of interannual variability (Tang et al., 2004, 2005; Chen et al., 2004; Tang et al., 2008).

The observed Niño3 SSTA index and predicted counterpart values by Scheme 3 are displayed in Fig. 9 for the period from 1876 to 2000. As can be seen, at a 6-month lead the model was able to predict most of warm and cold events, especially for relatively strong ENSO events, although the predicted SSTA always leads to the observed counterpart by 1–2 months. The phase shift between

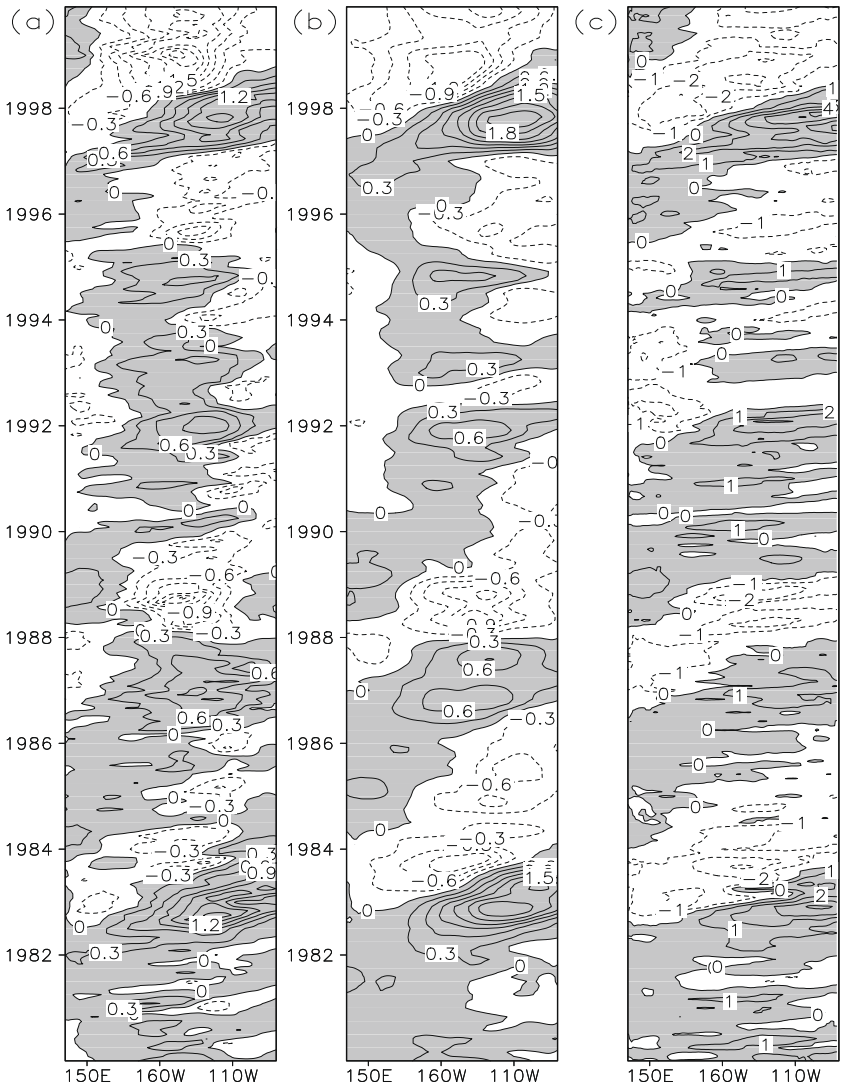

Fig. 6. Time-longitude plots of the second-layer temperature anomalies along the equator during 1980–2000 for (a) control experiment, (b) data assimilation of Scheme 3, and (c) data assimilation of Scheme 4. The contour level is 0.03 in (a) and 0.2 in (b) and (c). The values over 0 °C are shaded.

prediction and observation is due to the oceanic model's systematic bias, which also exists in other oceanic models, and in the control run where the observed winds are only forced with the oceanic model (Tang et al., 2001).

6. Discussion and conclusion

In this study, we proposed four schemes for the assimilation of the historic SST data based on different representations of the BEC. The BEC is a critical component in the data assimilation and determines how to spread the information of the observed SST in both horizontal and vertical directions. These schemes were compared based on the ocean analyses and ENSO prediction skills. Scheme 1 defines the BEC by a simple Gaussian function as in Derber and Rosati (1989), and the BEC in Schemes 2 and 3 is constructed based on modeled temperature of the control run forced by the observed wind stresses. Scheme 1 and 2 fail to correct the second-layer temperature directly, leading to little corrections in the second-layer temperature during the assimilation cycle. This suggests that the SST correction cannot transfer effectively to the subsurface by the model itself. Thus for the SST assimilation, the error vertical structure must be considered in the BEC. By considering spatial coherence in both horizontal and vertical directions and the location-dependent correlation scales of model errors, Scheme 3 produces the most realistic characteristics in the second-layer temperature than the others. Although the same BEC is used in both Schemes 3 and 4, the interannual variability of subsurface temperature in Scheme 4 is less realistic than Scheme 3 due to a proxy data used in Scheme 4. In terms of the prediction of Niño3 SSTA indices, the Scheme 3 also is the best among four schemes, suggesting that it is appropriate to estimate horizontal and vertical correlation scales of model errors using the model outputs as proposed in this study.

Long-term hindcasts were performed for the period from 1876 to 2000, initialized by data assimilation and the control run, respectively. The results show that the prediction skills of Niño3 SSTA index initialized by Scheme 3 are much better than those initialized by the control run and other assimilation schemes. For the first 20 years from 1876 to 1895 and the last 60 years from 1941 to 2000, the correlation coefficients initialized by Scheme 3 are around 0.5 at the 12-month lead, which are comparable with some best prediction models (e.g., Chen et al., 2004; Tang et al., 2008). A detail comparison of prediction skills for three different coupled models can be found in Tang et al. (2008). However, prediction skills initialized by either Scheme 3 or the control run are poor

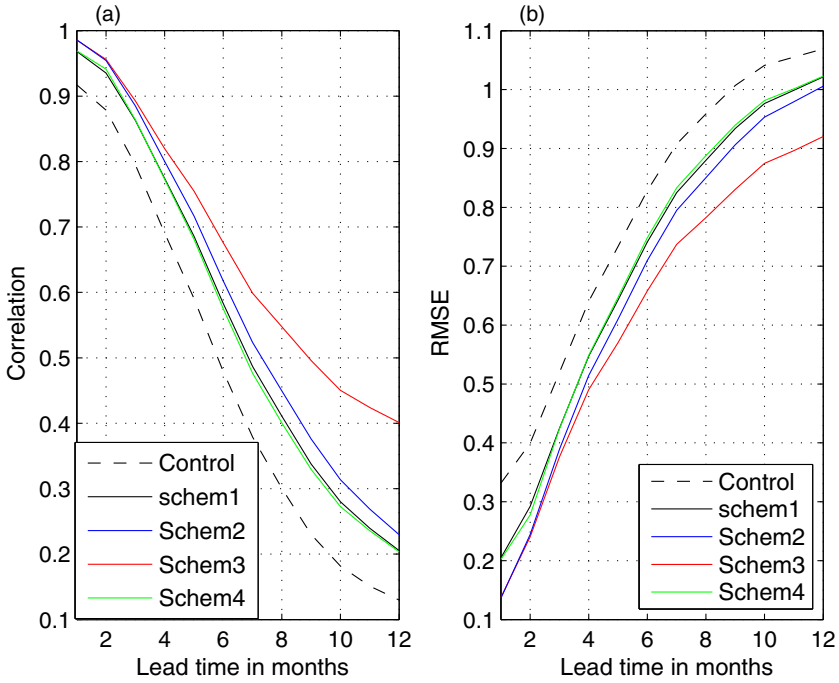

Fig. 7. (a) Correlation and (b) RMSE between observed and predicted Niño3 SSTA, as a function of lead time. The predictions are initialized every 3 months from April 1, 1876 to January 1, 2000. The dashed and solid lines are, respectively, for the predictions initialized from the control experiment and the ocean analyses with data assimilation.

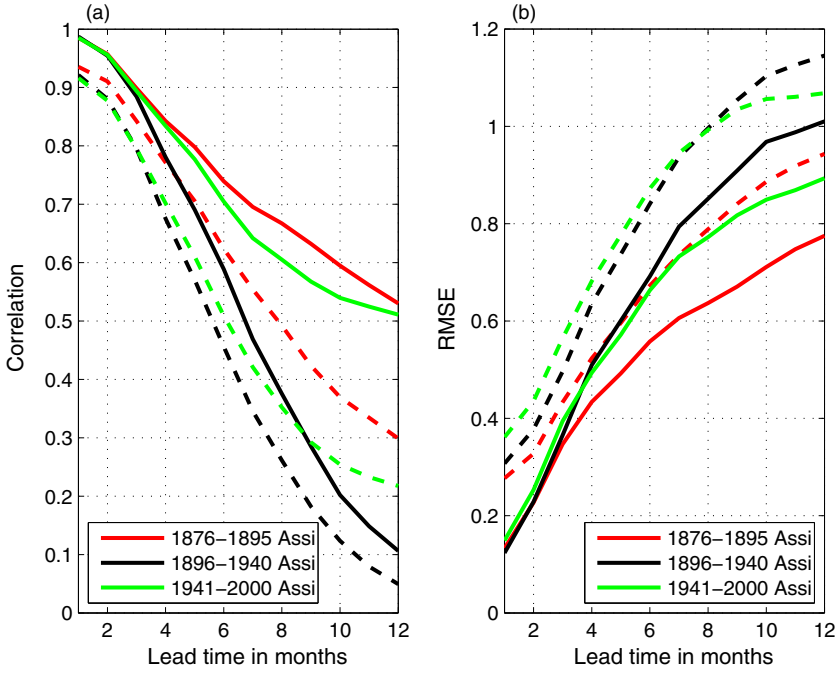

Fig. 8. (a) Correlation and (b) RMSE between observed and predicted Niño3 SSTA, as a function of lead time. The predictions are initialized every 3 months from April 1, 1876 to January 1, 2000. The dashed and solid lines are from the predictions initialized from the control experiment and ocean analyses by Scheme 3, respectively. The different color represents the different period. (For interpretation of the references to color in this figure legend, the reader is referred to the web version of this article.)

for the period 1896–1940, especially for the lead time beyond 7 months, clearly demonstrating a decadal-scale variation of ENSO predictability. Interestingly, the decadal variation of ENSO prediction skills shown in our model is very consistent with that found in Lamont model (Chen et al., 2004), suggesting that the decadal variation of ENSO predictability could be model independent. A further analysis found that the period of low predictability has very weak interannual variability. This is very consistent with several recent works on ENSO predictability which argued the amplitude of initial conditions dominating the prediction skill (e.g., Tang et al., 2004, 2005).

An important issue in surface data assimilation is the imbalance between the fast corrections in the surface and slow adjustments in the subsurface. This work aims at this issue by considering SST assimilation, a unique long-term oceanic dataset available, for initializing ENSO prediction. Thus, this work has both theoretical and

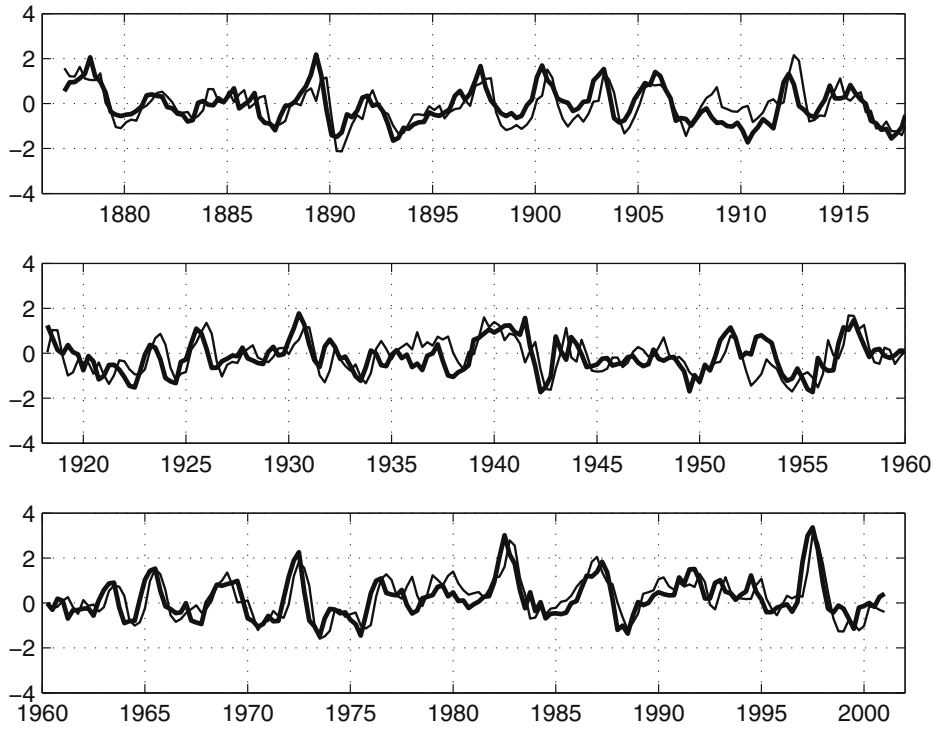

Fig. 9. Variation of the predicted Niño3 SSTA index of the 6-month lead (thin line) and the observed Niño3 SSTA index (thick line).

practical importance. Especially, some ENSO models with intermediate complexity can well simulate SSTA variations, but poorly simulate subsurface temperature. A direct assimilation of subsurface observations could lead to a large shock to models, destroying physics and dynamics of the models. In this sense, even though the subsurface observations are available, their direct assimilations might not be effective for these simplified models. In this study, we proposed and developed an alternative method that corrects model subsurface temperature by model SSTA increments. This proposed method might be able to solve the imbalance induced in the salinity field when the temperature is assimilated. For example, one could calculate the cross-covariance of model temperature and salinity errors from the control run, and then use it to transfer the SST increment into the salinity field. Further study and application of BEC into a global oceanic general circulation model is under way.

It should be noted that the SST observations represent typically the first few centimeters but the model SST is measured at the first-layer of this model with a reference depth of 100 m. Thus an inconsistence exists between model SST and the observed counterparts. This is a common and well known difficulty when assimilating SST, especially for a model with coarse resolution in vertical. Thus the achievement by SST assimilation shown in this study is probably a lower bound of the potential improvement of SST assimilation to oceanic analysis and ENSO prediction.

Acknowledgments

This work was supported by the Discovery grant of Natural Sciences and Engineering Research Council (NSERC) of Canada and BC-China Innovation and Commercialization Strategic Development Program Grant ICSD-2007-Tang-Y. We thank two anonymous reviewers for their constructive comments. The author X.Z. wishes to thank Dr. Guangqing Zhou for his helpful discussions.

References

Alves, O., Robert, C., 2005. Tropical Pacific Ocean model error covariances from Monte Carlo simulations. Quart. J. Roy. Meteorol. Soc. 131 (613), 3643–3658.
Anderson, D.L.T., McCreary, J.P., 1985. Slowly propagating disturbances in a coupled ocean–atmosphere model. J. Atmos. Sci. 42, 615–629.
Balmaseda, M., Anderson, D.L.T., Davey, M.K., 1994. ENSO prediction using a dynamical ocean model coupled to statistical atmospheres. Tellus 46A, 497–511.
Balmaseda, M., Davey, M.K., Anderson, D.L.T., 1995. Decadal and seasonal dependence of ENSO prediction skill. J. Climate 8, 2705–2715.
Behringer, D.W., Ji, M., Leetmaa, A., 1998. An improved coupled model for ENSO prediction and implication for ocean initialization. Part I: the ocean data assimilation system.. Mon. Wea. Rev. 126, 1013–1021.
Borovikov, A., Rienecker, M.M., Keppenne, C.L., Johnson, G.C., 2005. Multivariate error covariance estimates by Monte Carlo simulation for assimilation studies in the Pacific Ocean. Mon. Wea. Rev. 113, 2310–2334.
Cane, M.A., Zebiak, S.E., Dolan, S.C., 1986. Experimental forecasts of El Nino. Nature 321, 827–832.
Chen, D., Zebiak, S.E., Busalacchi, A.J., Cane, M.A., 1997. Initialization and predictability of a coupled ENSO forecast model. Mon. Wea. Rev. 125, 773–788.
Chen, D., Cane, M.A., Kaplan, A., Zebiak, S.E., Huang, D., 2004. Predictability of El Niño in the past 148 years. Nature 428, 733–736.
Deng, Z., Tang, Y., 2009. Reconstructing the past wind stresses over the tropical Pacific Ocean from 1875 to 1947. J. Appl. Meteorol. Climatol. 48 (6), 1181–1198.
Derber, J., Rosati, A., 1989. A global oceanic data assimilation system. J. Phys. Oceanogr. 19 (9), 1333–1347.
Fisher, M., Courtier, P., 1995. Estimating the covariance matrix of analysis and forecast error in variational data assimilation. ECMWF Technical Memorandum No. 220.
Hollingsworth, A., Lonnberg, P., 1986. The statistical structure of short-range forecast errors as determined from radiosonde data. Part I: the wind field. Tellus 38A, 111–136.
Kalnay, E. et al., 1996. The NCEP/NCAR 40-year reanalysis project. Bull. Am. Meteorol. Soc. 77, 437–470.
Kaplan, A., Cane, M., Kushnir, Y., Clement, A., Blumenthal, M., Rajagopalan, B., 1998. Analyses of global sea surface temperature 1856–1991. J. Geophys. Res. 103, 18567–18589.
Keenlyside, N., Latif, M., Botzet, M., Jungclaus, J., Schulzweida, U., 2005. A coupled method for initializing El Niño Southern Oscillation forecasts using sea surface temperature. Tellus 57A (3), 340–356.
Kug, J., Kang, I., Jhun, J., 2005. Western Pacific SST prediction with an intermediate El Niño prediction model. Mon. Wea. Rev. 133, 1343–1352.
Lorenc, A.C., 1986. Analysis methods for numerical weather prediction. Quart. J. Roy. Meteorol. Soc. 112, 1177–1194.
Luo, J., Masson, S., Behera, S., Shingu, S., Yamagata, T., 2005. Seasonal climate predictability in a coupled OAGCM using a different approach for ensemble forecasts. J. Climate 18, 4474–4497.

Martin, M.J., Hines, A., Bell, M.J., 2007. Data assimilation in the FOAM operational short-range ocean forecasting system: a description of the scheme and its impact. Quart. J. Roy. Meteorol. Soc. 133, 981–995.
Monahan, A.H., Dai, A., 2004. The spatial and temporal structure of ENSO nonlinearity. J. Climate 17, 3026–3036.
Nakaegawa, T., Kanamttsu, M., Smith, T.M., 2004. Interdecadal trend of prediction skill in an ensemble AMIP-type experiment. J. Climate 15, 2881–2889.
Oke, P.R., Schiller, A., Griffin, G.A., Brassington, G.B., 2005. Ensemble data assimilation for an eddy-resolving ocean model. Quart. J. Roy. Meteorol. Soc. 131, 3301–3311.
Oke, P.R., Brassington, G.B., Griffin, D.A., Schiller, A., 2008. The Bluelink Ocean Data Assimilation System (BODAS). Ocean Modell. 20, 46–70. doi:10.1016/j.ocemod.2007.11.002.
Parrish, D.F., Derber, J., 1992. The National Meteorological Center's spectral statistical interpolation analysis system. Mon. Wea. Rev. 120, 1747–1763.
Rosati, A., Miyakoda, K., Gudgel, R., 1997. The impact of ocean initial conditions on ENSO forecasting with a coupled model. Mon. Wea. Rev. 125, 754–772.
Shinoda, T., Hendon, H.H., 1998. Mixed layer modeling of intraseasonal variability in the tropical western Pacific and Indian oceans. J. Climate 11, 2668–2685.
Smith, T.M., Reynolds, R.W., 2003. Extended reconstruction of global sea surface temperatures based on COADS data (1854–1997). J. Climate 16, 1495–1510.
Smith, T.M., Reynolds, R.W., 2004. Improved extended reconstruction of SST (1854–1997). J. Climate 17, 2466–2477.
Tang, Y., 2002. Hybrid coupled models of the tropical Pacific – interannual variability. Climate Dyn. 19, 331–342.
Tang, Y., Hsieh, W.W., 2003. ENSO simulation and predictions using a hybrid coupled model with data assimilation. J. Jpn. Meteorol. Soc. 81 (1), 1–19.
Tang, Y., Kleeman, R., 2002. A new strategy for SST assimilation for ENSO prediction. Geophys. Res. Lett. doi:10.1029/2002GL014860.
Tang, Y., Hsieh, W.W., Tang, B., Haines, K., 2001. A neural network atmospheric model for hybrid coupled modelling. Climate Dyn. 17, 445–455.
Tang, Y., Kleeman, R., Moore, A., 2004. SST assimilation experiments in a tropical Pacific Ocean model. J. Phys. Oceangr. 34 (3), 623–642.
Tang, Y., Kleeman, R., Moore, A., 2005. On the reliability of ENSO dynamical predictions. J. Atmos. Sci. 62 (6), 1770–1791.
Tang, Y., Deng, Z., Zhou, X., Cheng, Y., Chen, D., 2008. Interdecadal variation of ENSO predictability in multiple models. J. Climate 21, 4811–4833.
Weaver, A., Courtier, P., 2001. Correlation modelling on the sphere using a generalized diffusion equation. Quart. J. Roy. Meteorol. Soc. 127 (575), 1815–1846.
Xue, Y., Smith, T.M., Reynolds, R.W., 2003. Interdecadal changes of 30-yr SST normals during 1871–2000. J. Climate 15, 1601–1612.
Zebiak, S.E., Cane, M.A., 1987. A model El Niño–Southern Oscillation. Mon. Wea. Rev. 115, 2262–2278.
Zhou, G., Fu, W., Zhu, J., Wang, H., 2004. The impact of location-dependent correlation scales in ocean data assimilation. Geophys. Res. Lett. 31, L21306. doi:10.1029/2004GL020579.